RSC Medicinal Chemistry



RESEARCH ARTICLE

View Article Online



Cite this: RSC Med. Chem., 2025, 16, 3633

Development and clinical potential of ¹⁸F-PSiMA for prostate cancer PET imaging†

Lexi Gower-Fry, (1) ‡a Justin J. Bailey, ‡§b Melinda Wuest, b Susan Pike, b Alexey Kostikov, (Dcd Andreas Dorian, Ta Carmen Wängler, (Def Frank Wuest and Ralf Schirrmacher*ab

Prostate-specific membrane antigen (PSMA) is a key target for diagnosing prostate cancer through positron emission tomography (PET). While ⁶⁸Ga-labeled PSMA compounds are widely used, ¹⁸F-labeled PSMA inhibitors have gained traction for clinical tumor imaging. We previously investigated PSMA-targeting compounds based on the Lys-urea-Glu motif, incorporating a silicon fluoride-acceptor (SiFA) and chemical auxiliaries to enhance in vivo biodistribution. This led to the development of ¹⁸F-PSiMA, a SiFA-based radiotracer with an optimized linker exhibiting favorable PSMA potency (IC_{50} = 154 \pm 47 nM in LNCaP cells). ¹⁸F-PSiMA radiosynthesis with low to high concentrations of ¹⁸F and precursor achieved molar activities (A_m) of 10.9–82.5 GBg μ mol⁻¹ and showed a 24–38% increase in tumor uptake in LNCaP tumors $(SUV_{60min} 1.56 \pm 0.18; 7.23 \pm 0.75\% ID per g at lower A_m and <math>SUV_{60min} 1.90 \pm 0.29; 9.62 \pm 1.29\% ID per g$ at higher A_m) compared to our previous lead, ¹⁸F-SiFA-Asp₂-PEG₃-PSMA. PSMA specificity was confirmed by a 20 \pm 10% reduction in SUV_{60min} upon co-injection with DCFPyl. These promising in vitro and in vivo results support further clinical translation of ¹⁸F-PSiMA for prostate cancer PET imaging.

Received 31st March 2025. Accepted 6th May 2025

DOI: 10.1039/d5md00275c

rsc.li/medchem

Introduction

The detection of recurrent and metastatic prostate cancer is important for disease staging and planning an effective treatment regimen. Recent developments and combinations of different molecular imaging modalities such as positron emission tomography (PET) and magnetic resonance imaging (MRI) have led to an improved diagnosis and prognostic outcome for prostate cancer patients.^{1,2} Radiotracers targeting prostate-specific membrane antigen (PSMA), a glycoprotein that is highly overexpressed in prostate cancer, have significantly enhanced the diagnosis of this disease across different disease stages.3 The staging of high-risk prostate

cancer, particularly in assessing biochemical recurrence in castration-resistant prostate cancer (CRPC), has greatly benefited from a wide range of clinically used PET and singlephoton emission computed tomography (SPECT) radiotracers that target PSMA.4

Recently, it has been clinically established that PSMA imaging is most beneficial to patients diagnosed early with intermediate to very-high-risk prostate cancer as well as biochemical recurrence and CRPC.3,4 Molecular imaging of PSMA using radiotracers bearing the structural Lys-urea-Glu motif provide the radiopharmacological tools for tumor staging and dosimetry for radionuclide-based prostate cancer therapy. 5-8 Over the past decade an impressive variety of PSMAbinding tracers have been introduced into the clinic, most of which were either labeled with gallium-68 (68 Ga, $t_{1/2}$ = 68 min), a typically generator-produced radionuclide, or fluorine-18 (18F, $t_{1/2}$ = 110 min), a cyclotron-based nuclide. All these compounds are small molecule inhibitors binding to the extracellular domain of PSMA. The synthesis of a diverse range of structurally similar compounds based on the Lys-urea-Glu motif has led to significant clinical advancements, resulting in FDA approvals for ⁶⁸Ga-PSMA-11, ¹⁸F-DCFPyl, and most recently, 18F-rhPSMA-7.3.9-11 The latter is a radiohybrid radiotracer which utilizes the silicon fluoride-acceptor (SiFA) technology for 18F-radiolabeling, while also containing a DOTAGA chelator for labeling with ⁶⁸Ga or therapeutic radiometals. A range of promising PSMA-targeting radiotracers,

^a Department of Chemistry, University of Alberta, Edmonton, Alberta, Canada. E-mail: schirrma@ualberta.ca

^b Department of Oncology, University of Alberta, Edmonton, Alberta, Canada

^c Department of Neurology and Neurosurgery, McGill University, Montreal, Quebec,

^d Department of Chemistry, McGill University, Montreal, Quebec, Canada

^e Biomedical Chemistry, Clinic of Radiology and Nuclear Medicine, Medical Faculty Mannheim, Heidelberg University, Germany

f Research Campus M2OLIE, Medical Faculty Mannheim, Heidelberg University,

[†] Electronic supplementary information (ESI) available. See DOI: https://doi.org/ 10.1039/d5md00275c

[†] These authors contributed equally.

⁸ Current address: TRIUMF, Vancouver, BC, Canada,

[¶] Current address: 48 Hour Discovery, Edmonton, AB, Canada.

including ¹⁸F-PSMA-1007, ⁶⁸Ga-PSMA-16 and ⁶⁸Ga-PSMA-I&T, are currently in clinical trials, expanding the scope of diagnostic agents for PSMA imaging. 5,12,13 Recently disclosed ¹⁸F-labeled tracers such as ¹⁸F-CTT1057, ¹⁸F-JK-PSMA-7, ¹⁸F-FSU-880 and ¹⁸F-AlF-PSMA-11 suggest a shift from ⁶⁸Ga-labeled tracers to ¹⁸F-fluorinated radiopharmaceuticals, driven by the superior imaging resolution of ¹⁸F-based radiopharmaceuticals and the high cost and limited availability of approved ⁶⁸Ge/ ⁶⁸Ga-generator systems. ^{14–17}

Research Article

The SiFA labeling concept, which utilizes isotopic exchange (IE) of nascent F-19 with [18F]fluoride, represents an important addition to the expanding array of ¹⁸F-labeling techniques. This method has been validated for human molecular imaging applications, as demonstrated by the introduction of ¹⁸F-SiTATE, a somatostatin receptor-binding peptide labeled via the SiFA approach. 18-25 This peptide is clinically used in the diagnosis of neuroendocrine tumors, meningiomas, and, more recently, in cases of lenticulostriatal ischemia. 18-20,23,25-28 While advancing our line of SiFA-based PSMA radiotracers, we previously developed ¹⁸F-SiFA-Asp₂-PEG₃-PSMA (Fig. 1), our lead in the second generation of SiFA-PSMA radiotracers.²⁹ The first generation of SiFA-PSMA radiotracers consisted of the SiFA moiety and Lys-urea-Glu motif, with or without a PEG linker. 29 18F-SiFA-Asp2-PEG3-PSMA (Fig. 1), with an IC₅₀ of 125 nM, demonstrated the highest LNCaP tumor uptake among nine novel SiFA-bearing PSMA inhibitors when injected with a molar activity (A_m) of up to 86 GBq μmol⁻¹.²⁹ Its uptake into LNCaP tumor bearing mice was favorable with an SUV_{60min} of 1.18, comparable to that of ¹⁸F-PSMA-1007.^{5,29}

In our previous investigations into structural auxiliaries to enhance SiFA-based imaging agents (e.g. 18F-SiTATE), we identified several factors that influence biodistribution and non-specific binding. Key modifications, including the incorporation of aspartic acid, a PEG linker, and a positively charged ammonium group, were found to mitigate the inherently high lipophilicity of the SiFA functionality. 27,29-31 This lipophilicity can negatively affect biodistribution, leading to elevated hepatobiliary clearance and non-specific binding.³² Notably, the addition of a quaternary ammonium group significantly influenced these parameters, reducing non-specific binding and improving overall biodistribution.

For the radiotracers ¹⁸F-SiTATE and ¹⁸F-SiFA-Asp₂-PEG₃-PSMA (Fig. 1), these modifications successfully redirected clearance towards a more renal clearance pathway. 29,31 However, ¹⁸F-SiFA-Asp₂-PEG₃-PSMA still exhibited nonspecific muscle uptake, which we hypothesized could be further reduced by decreasing the radiotracer's ability to passively diffuse through cell membranes.²⁹ While PEG groups had minimal impact on tumor uptake compared to aspartic acid, the introduction of a quaternary ammonium salt showed promise in significantly enhancing the tumor-tobackground ratio. A permanently positively charged motif was previously shown to decrease the lipophilicity of a SiFAbearing molecule by a factor of 8, while retaining biological stability and high radiochemical yield (RCY) from the IE reaction with [18F]fluoride.30 The incorporation of the quaternary ammonium moiety alongside two aspartic acids, previously reported in ¹⁸F-SiTATE, resulted in higher tumor uptake, better tumor-to-background tissue ratios, and superior image quality compared to the gold standard, ⁶⁸Ga-DOTATATE. 21,27,31

Building on these findings, we have now synthesized ¹⁸F-PSiMA (18F-14, Fig. 1), our third generation radiotracer designed on a Lys-urea-Glu framework. This novel compound incorporates two aspartic acid groups, a quaternary ammonium group, and an alkyl linker, optimizing its structure for enhanced performance. To support its development, we established an efficient SiFA radiolabeling IE procedure, refined a robust purification protocol, and conducted comprehensive evaluations of 18F-PSiMA both in vitro and in vivo using the PSMA-expressing LNCaP prostate cancer model. These efforts underscore ¹⁸F-PSiMA's potential as a next-generation diagnostic tool in prostate cancer imaging.

Results and discussion

The 19F-PSiMA, 14 (Fig. 1), was synthesized following a protocol similar to previously reported methods, from three building blocks: the SiFA-Asp₂ tag 3, a quaternary ammonium linker 7, and the Lys-urea-Glu targeting moiety 11 (Scheme 1).²⁹ To construct the SiFA-Asp₂ tag 3, an SiFA-NHS active ester 1 underwent an amidation reaction with t-butyl protected aspartic acid to produce SiFA-Asp₁ intermediate 2 in 33% yield. A second aspartic acid was attached in a two-step method, first generating an activated ester using EDCI/NHS, followed by the addition of H-L-Asp(OtBu)-OH, to give the SiFA-Asp2 building block 3 in 52% yield after HPLC purification.

Fig. 1 Structure of the previous second generation lead SiFA-PSMA radiotracer, ^{18/19}F-SiFA-Asp₂-PEG₃-PSMA, compared to the novel third generation radiotracer, ^{18/19}F-PSiMA (^{18/19}F-**14**).

Scheme 1 Synthesis of PSiMA building blocks. ^aReagents and conditions: (a) H-L-Asp(OtBu)-OH, DIPEA, DMF, 33%; (b) step 1. NHS, EDCI, DMF, step 2. H-L-Asp(OtBu)-OH, DMF 26% over two steps; (c) NaN₃, deionized H₂O, 80 °C, 86%; (d) 2-(Boc-amino)ethyl bromide, MeCN; (e) 2 M HCl, Et₂O, 71% over two steps; (f) step 1. *P*-Nitrophenyl chloroformate, DIPEA, CH₂Cl₂; step 2. H-Lys(Z)-OtBu, 86% over two steps; (g) H₂, Pd/C, MeOH, 88%; (h) 10-undecynoic acid, HBTU, DIPEA, DMF, 70%.

The quaternary ammonium linker 7 was synthesized with an azide and an amine moiety for orthogonal coupling to the SiFA-Asp₂ 3 and an alkyne-functionalized Lys-urea-Glu 11, respectively. Heating commercially available 2-chloro-*N*,*N*-dimethylethan-1-aminium chloride 4 in deionized water with sodium azide provided intermediate 5. Alkylation of 5 with *N*-Boc-2-bromoethyl-amine yielded 6, and subsequent deprotection using 2 M HCl in diethyl ether, gave the final quaternary ammonium building block 7, with a 71% yield, over two steps.

The PSMA binding motif, Lys-urea-Glu, was also retained in the structure of PSiMA. Synthesis of the Lys-urea-Glu PSMA binding motif **10** proceeded as previously reported *via* the cross-coupling of two commercially available *tert*-butyl- and CBZ-protected amino acids, H-Glu(OtBu)-OtBu **8** and H-

Lys(Z)-OtBu, to produce intermediate $9.^{29,33,34}$ CBZ-deprotection using Pd/C hydrogenolysis provided the free amine 10 in 88% yield.

A hydrophobic linker adjacent to the PSMA-targeting motif was previously shown in literature to improve the binding affinity up to 60-fold due to its interactions with a lipophilic pocket a short distance away from the active site of PSMA. This also had a positive effect on the tumor uptake of PSMA radiotracers in LNCaP-tumor bearing mice. Therefore, a hydrophobic alkyl linker was utilized in the synthesis of 14. 10-undecynoic acid was converted to active ester with HBTU, then a coupling reaction was performed with the primary amine 10 to provide the Lys-urea-Glu building block 11 in 70% yield.

Synthesis of 14 was achieved through coupling of the SiFA-Asp₂ 3 carboxylic acid with the amine handle of the

Scheme 2 Synthesis of 18 F-PSiMA. a Reagents and conditions: (i) 7, HBTU, DIPEA, DMF, 95%; (j) 11, CuSO₄, sodium ascorbate, THF; (k) 1:1 TFA/CH₂Cl₂, 20% over two steps; (l) 18 F]fluoride, K₂₂₂, K₂CO₃, MeCN.

quaternary ammonium linker 7 (Scheme 2). To overcome solubility issues of 7, sonication and heat were utilized to assist the reaction. The SiFA-Asp₂-QA intermediate 12 was successfully synthesized in 95% yield after HPLC purification. SiFA-Asp₂-QA 12 was coupled to the Lys-urea-Glu alkyne via copper catalyzed alkyne-azide cycloaddition (CuAAC) to yield tert-butyl protected PSiMA 13. Without purification, the solvent was removed and a 1:1 mixture of TFA and CH₂Cl₂ was added for the final tert-butyl deprotection. After the deprotection, purification by HPLC gave the final product 14 in 20% yield, over two steps.

Research Article

The radiosynthesis of ¹⁸F-PSiMA was realized through ¹⁹F-¹⁸F IE of the SiFA moiety. To achieve this, the "four-drop method" was used to elute the [18F]fluoride from the QMA solid phase cartridge minimizing the amount of base in the reaction, obviating the use of oxalic acid to manage pH as with other SiFA labeling protocols.³⁶ The final product, ¹⁸F-PSiMA, was obtained with an $A_{\rm m}$ of 10.93 \pm 3.70 GBq $\mu {\rm mol}^{-1}$ (n = 6), in 13 ± 8% radiochemical yield (RCY) (n = 6)uncorrected for radioactive decay). The total synthesis time was 90 min (from time of drying to formulation) and >99% radiochemical purity (RCP) was determined through quality control (QC) radio-HPLC.

The $\log D_{7.4}$ of ¹⁹F-PSiMA was determined as <-3, thus more hydrophilic than ¹⁸F-PSMA-1007 with -1.6, and similar to the previously reported second generation lead SiFA-PSMA radiotracer, 19 F-SiFA-Asp₂-PEG₃-PSMA, with a $\log D_{7.4}$ of -3.03as well as 19 F, $^{\text{nat}}$ Ga-rhPSMA-7.3 $\log D_{7.4}$ of $-3.2.^{29,37,38}$ A hydrolytic stability assay performed under physiological conditions (pH 7.4 and 37 °C) showed that ¹⁹F-PSiMA is sufficiently stable for in vivo application with very slow hydrolysis to the silanol ($t_{1/2}$ of 177 \pm 3 h).

Competitive displacement experiments in PSMA-expressing LNCaP cells revealed an IC₅₀ value of 154 \pm 47 nM (Fig. 2A, n=6/2) which was similar to SiFA-Asp₂-PEG₃-PSMA (IC₅₀ = 125 nM). 29 18 F-PSiMA uptake into LNCaP cells resulted in 36 \pm 8% radioactivity/mg protein (n = 6/2) after 120 min incubation time (Fig. 2B). An in vitro blocking study with inhibitor compound 2-PMPA resulted in 75% blocking of LNCaP cell uptake (Fig. 2C). Additionally, it was determined through a glycine wash of the LNCaP cells that ~68% of the radiotracer is internalized (Fig. 2D, n = 6/1). Uptake into LNCaP prostate tumors in vivo was ~24% higher compared to the previous analogue, ¹⁸F-SiFA-Asp₂-PEG₃-PSMA (Fig. 3A and D, SUV_{60min} 1.56 ± 0.18 corresponding to $7.23 \pm 0.75\%$ ID per g (n = 3) versus 1.18 ± 0.12 and $5.64 \pm 0.35\%$ ID per g (n = 3) for ¹⁸F-SiFA-Asp₂-PEG₃-PSMA), despite having a significantly lower $A_{\rm m}$ (10.9 GBq $\mu \text{mol}^{-1} \nu s$. 86 GBq μmol^{-1}).²⁹ This tumor uptake was similar to that of 18 F-PSMA-1007 with 8.0 \pm 2.4% ID per g in mice, but lower than 18 F-rhPSMA-7.3 with 18.3 \pm 7.2% ID per g. 5,38 In vivo blocking studies using 300 µg of DCFPyL reduced tumor uptake by 20 \pm 10% to a SUV $_{60min}$ value of 1.24 \pm 0.06 (corresponding to 5.63 \pm 0.25% ID per g, n = 3) (Fig. 3D), which is similar to the 32% blocking effect with ¹⁸F-SiFA-Asp₂-PEG₃-PSMA.²⁹ Taken together, in vitro and in vivo blocking experiments have proven targeting efficacy of novel 18F-PSiMA despite some possible additional non-specific binding as experimentally observed.

For direct comparison with a leading clinical PSMAtargeting tracer, 18F-PSMA-1007 was obtained from the

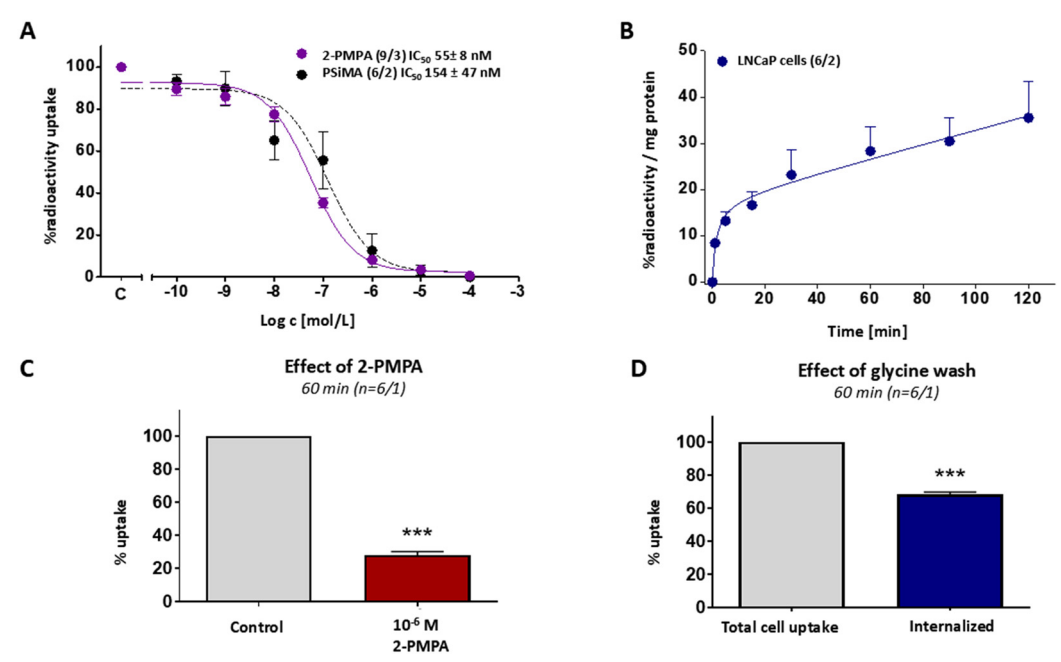


Fig. 2 A) Inhibition-response curve against 18 F-PSMA-1007. Data are shown as mean \pm SEM from n = 6-9 data points from 1–2 experiments. B) In vitro LNCaP cell uptake of 18 F-PSiMA over 120 min. Data are shown as mean \pm SEM from n=6 datapoints from two experiments. C) Blocking of in vitro 18 F-PSiMA cell uptake with PSMA inhibitor 2-PMPA (1 μ M). Data are shown as mean \pm SEM from n=6 data points from one experiment. D) 18 F-PSiMA internalization into LNCaP cells. Data are shown as mean \pm SEM from n=6 data points from one experiment.

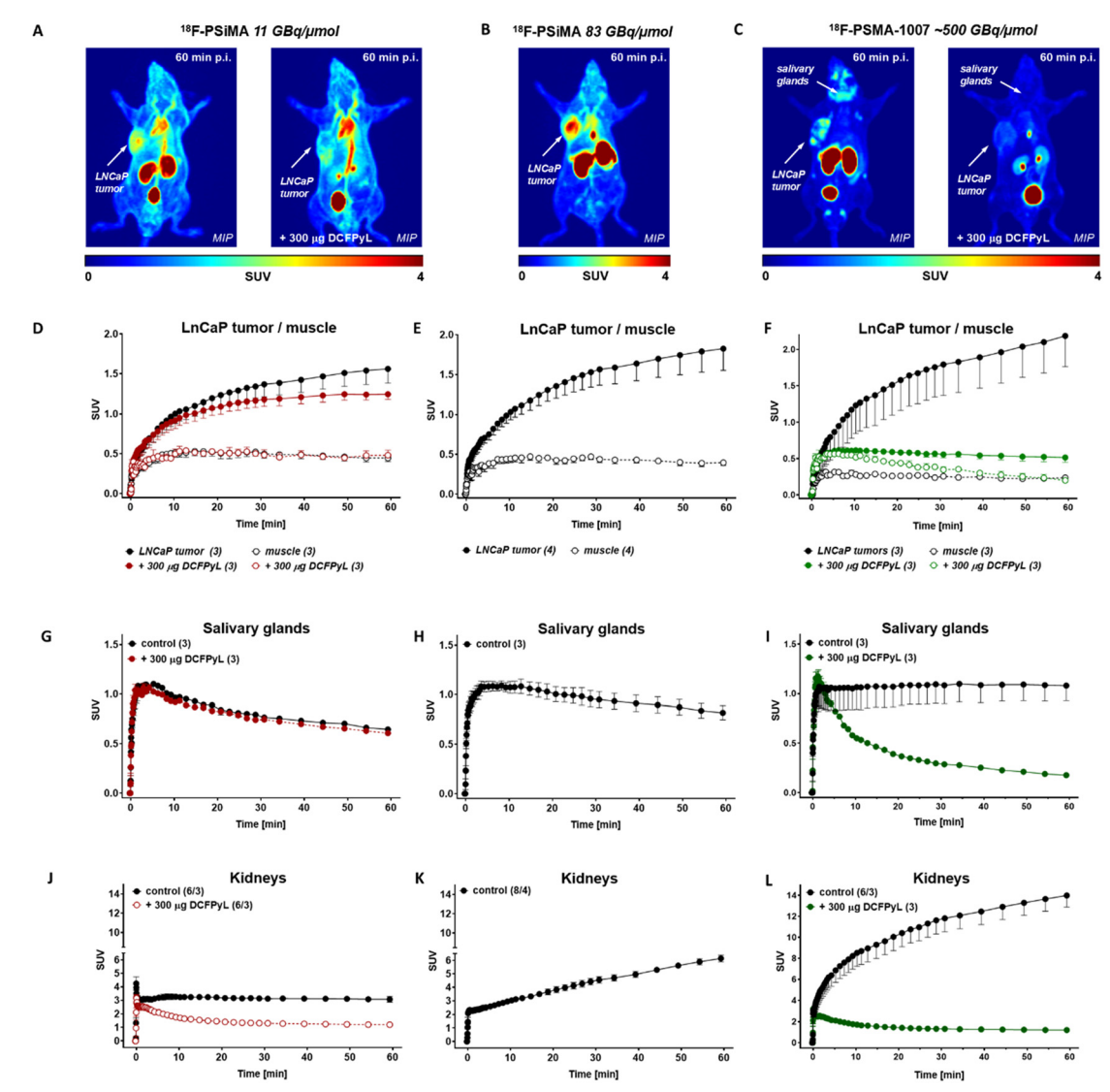


Fig. 3 Representative PET images as maximum intensity projections (MIP) of novel ¹⁸F-PSiMA (A and B) and ¹⁸F-PSMA-1007 (C) in LNCaP-tumor bearing mice at 60 min post injection. Corresponding time-activity curves (TACs) for radiotracer uptake into LNCaP tumor and muscle tissue (D-F) the salivary glands (G-I) and kidneys (J-L) in the absence and presence of 300 μ g blocking DCFPyL. Data are shown as mean \pm SEM from n=3, n=1= 4 experiments.

routine clinical production done by the Edmonton Radiopharmaceutical Centre (ERC). The novel SiFA-PSMA compound 18F-PSiMA had a longer blood circulation time compared to clinical 18F-PSMA-1007, as well as a delayed non-target tissue and background clearance. However, it

is not taken up by the salivary glands, resulting in a more prostate-specific binding to PSMA (Fig. 3G and I). This prostate-specific target binding is also supported by an around 4-fold lower kidney uptake (Fig. 3J and L), as mouse kidney tissue also express PSMA receptors.³⁹

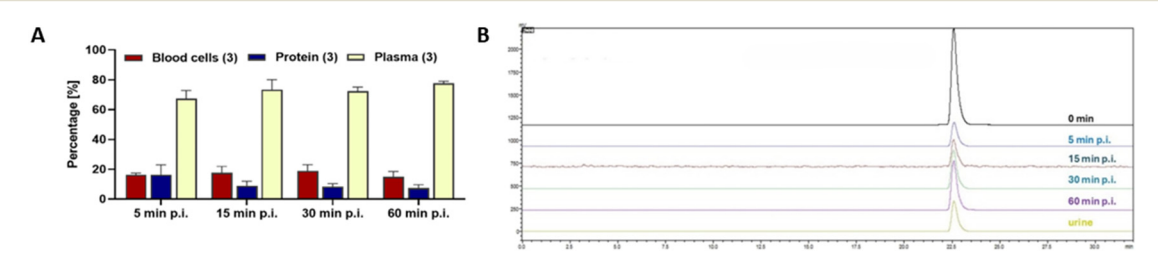


Fig. 4 A) Blood cell compartment distribution of 18 F-PSiMA. Data are shown as mean \pm SEM from n=3 experiments. B) In vivo metabolic stability of ¹⁸F-PSiMA in normal control mouse. Representative HPLC chromatograms from blood plasma & urine samples.

Blocking with DCFPyL confirmed PSMA binding of ¹⁸F-PSiMA and ¹⁸F-PSMA-1007 in PSMA expressing mouse kidney tissue (Fig. 3J and L), while blocking PSMA in salivary glands was detected with ¹⁸F-PSMA-1007 only (Fig. 3G and I). *In vivo* metabolism analysis revealed a 67–78% plasma availability and 7–16% protein binding of ¹⁸F-PSiMA over 5 to 60 min post injection (Fig. 4). No radioactive metabolites were detectable in blood plasma or urine over the entire 60 min post injection (Fig. 4). Taken together, ¹⁸F-PSiMA represents a metabolically stable radiotracer *in vivo*.

Research Article

To increase $A_{\rm m}$, reaction parameters were optimized by reducing the precursor amount from 20 nmol to 5 nmol and increasing the starting activity of [18 F]fluoride from 1–1.5 GBq to 4.1 GBq. The reaction volume was reduced from 200 μ L to 50 μ L, and the reaction vial was preheated to 80 °C to facilitate faster reaction initiation. These modifications resulted in an $A_{\rm m}$ of 82.54 GBq μ mol $^{-1}$, with the resulting non-decay corrected RCY of 7.9% being slightly lower than the previous formulations of 13%.

In vivo PET imaging in LNCaP tumor-bearing mice, a well established PSMA-expressing prostate cancer model, 29,39 demonstrated a 38% higher tumor uptake with the high $A_{\rm m}$ 18 F-PSiMA tracer (SUV $_{\rm 60min}$ 1.90 \pm 0.29; 9.62 \pm 1.29% ID per g (n=4)) (Fig. 3B and E) compared to the lower $A_{\rm m}$ formulation (10.93 GBq μ mol $^{-1}$). Interestingly, no radioactivity was observed in the bladder with the higher $A_{\rm m}$ tracer, with all radioactivity localized to the kidneys. This altered biodistribution suggests a potential pharmacological blocking of the renal uptake pathways at lower $A_{\rm m}$, leading to increased kidney clearance of the radioactivity. While the precise mechanism remains unclear, this observation aligns with previous findings on PSMA-targeting radiotracers exhibiting kidney-specific binding due to PSMA receptor expression in renal tissue.

Given the large amount of radioactivity required to achieve a higher $A_{\rm m}$, further studies using high $A_{\rm m}$ ¹⁸F-PSiMA should be conducted following translation to an automated synthesis platform.

Overall, the novel ¹⁸F-PSiMA radiotracer demonstrates superior tumor uptake compared to previous analogues revealing it as a promising candidate for a potential clinical translation. Optimization of the radiosynthetic procedure and automation would further increase its potential as a clinical radiopharmaceutical.

Notably, ¹⁸F-PSiMA offers an advantage over ¹⁸F-PSMA-1007 due to its negligible salivary gland uptake and lower kidney tissue uptake. Additionally, the prolonged blood circulation time of ¹⁸F-PSiMA may lead to enhanced delivery of the radiotracer to the target site reaching an SUV_{60min} of 2.69 \pm 0.12 in the blood pool *versus* 0.37 \pm 0.04 for ¹⁸F-PSMA-1007 (both n=3; Fig. S1†). This represents a significant difference between both investigated ¹⁸F radiotracers.

Moreover, further investigation into the non-specific binding of SiFA-PSMA compounds is warranted and will be investigated in the future.

Conclusions

¹⁸F-PSiMA, our third generation SiFA-PSMA radiotracer, which incorporates two aspartic acids, a hydrophilic quaternary ammonium cation, and an alkyl linker, demonstrates a 24–38% increase in *in vivo* tumor uptake in LNCaP tumors compared to the second generation lead SiFA-PSMA radiotracer, ¹⁸F-SiFA-Asp₂-PEG₃-PSMA.

The significantly increased tumor uptake of 18F-PSiMA was accompanied by a negative side effect of enhanced nonspecific binding which could be reduced at higher $A_{\rm m}$. This was particularly evident in the blocking studies with DCFPyL, where the blocking effect was much smaller compared to 18F-PSMA-1007. Nevertheless, ¹⁸F-PSiMA exhibited negligible salivary gland uptake and a much lower kidney tissue uptake, offering a distinct advantage over clinically used 18F-PSMA-1007. This also indicates a potential for further optimization and development of a radiotherapeutic derivative of ¹⁸F-PSiMA. With additional optimization of the radiosynthesis and further investigation into the nature of the non-specific binding, tumor uptake may be further enhanced while reducing non-specific binding, offering a new foundation for development of SiFA-containing PSMA-targeting radiotracers.

Experimental

Materials and methods

Commercial reagents and solvents were purchased and used without further purification. 18F-PSMA-1007 was supplied by the Edmonton Radiopharmaceutical Centre (ERC) from routine clinical production. NMR spectra were recorded on a 700 Hz Agilent VNMRS four-channel, dual receiver spectrometer with a cryo-probe and 500 MHz Agilent/Varian VNMRS two-channel spectrometer with a 13C/1H dual cold probe. NMR spectra were calibrated in relation to the deuterated solvent signals. Multiplicities are indicated as s (singlet), d (doublet), dd (doublet of doublets), t (triplet), and m (multiplet). Analytical and semi-preparative HPLC (highperformance liquid chromatography) was conducted on an Agilent, Gilson, and Shimadzu with UV wavelength 254 nm radiodetector. HRMS (high-resolution mass spectrometry) was obtained using an Agilent Technologies 6220 oaTOF instrument. Purity of final compounds used for radiosynthesis, cell and animal studies were confirmed to be over 95% using HPLC.

Chemical synthesis

(*S*)-4-(*tert*-Butoxy)-2-(4-(di-*tert*-butylfluorosilyl)benzamido)-4-oxobutanoic acid (2). SiFA-NHS ester (1.58 g, 1.54 mmol), prepared according to literature, was combined with H-L-Asp(O*t*Bu)-OH (322 mg, 1.69 mmol) in a solution of DMF (19 mL) and DMSO (1 mL).²⁹ Hünig's base (92 μ L, 0.54 mmol) was added slowly and the resulting mixture was stirred for 20 hours at room temperature. The crude was concentrated under vacuum until only half the volume was left. The

solution was then combined with brine (150 mL) and extracted with CH_2Cl_2 (3 × 150 mL). The combined organic layers were dried over Na_2SO_4 , filtered, and concentrated under vacuum to afford a crude yellow oil. Purification by flash column chromatography (100% hexanes \rightarrow 100% EtOAc) gave compound 2 as a white powder in 33% yield (232 mg, mmol). R_f (6% MeOH in CH_2Cl_2) = 0.3. ¹H NMR (700 MHz, CDCl_3) δ 7.80 (d, 2H, J = 7.7 Hz), 7.69 (d, 2H, J = 7.0 Hz), 7.41 (d, 1H, J = 7.0 Hz), 5.07 (app. s, 1H), 3.07 (app. d, 1H, J = 14.7 Hz), 2.89 (app. d, 1H, J = 16.8 Hz), 1.44 (s, 9H), 1.04 (s, 18H, $\text{SiC}(\text{CH}_3)_3$); ¹³C NMR (176 MHz, CDCl_3) δ 175.0, 170.7, 167.5, 138.9 (d, J_{CF} = 13.4 Hz), 134.3, 134.3 (d, J_{CF} = 4.2 Hz), 126.2, 82.3, 49.2, 37.2, 28.0, 27.3, 20.2 (d, J_{CF} = 12.0 Hz). HRMS (ESI) m/z: [M - H] $^-$ calcd. For $\text{C}_{23}\text{H}_{35}\text{FNO}_5\text{Si}$ 452.2274, found 452.2262.

(2R)-4-tert-Butoxy-2-[[(2R)-4-tert-butoxy-2-[[4-[di-tert-butyl-(fluoro)silyl]benzoyl]amino]-4-oxo-butanoyl]amino]-4-oxobutanoic acid (3). Modified literature protocol was used to perform this reaction.²⁹ To a solution of 2 (200 mg, 0.441 mmol) in DMF (6 mL) was added N-hydroxysuccinimide (60.9 mg, 0.529 mmol) and 1-ethyl-3-(3-dimethylaminopropyl) carbodiimide (72 mg, 0.463 mmol). After 5 hours, H-L-Asp(OtBu)-OH (100 mg, 0.529 mmol) was added. The reaction was allowed to stir at room temperature for 19 h. The solvent was removed by co-evaporation with toluene, then diethyl ether was added and the white precipitate filtered off. The filtrate was washed with 10% NH₄Cl (15 mL), H₂O (15 mL × 2), and brine (15 mL). The aqueous combined fractions were back extracted with CH₂Cl₂ (15 mL × 3) and dried over Na₂-SO₄, filtered and concentrated under vacuum. The crude mixture was then purified via HPLC (C18(2) column: Luna 5 μ m 100 Å 250 mm × 10 mm; flow: 3 mL min⁻¹; solvent A: H₂O, solvent B: MeCN + 0.05% TFA, method: 0-5 min 70 to 85% B, 5-20 min 85% B, 20-21 min 80 to 85% B, 21-30 min 95% B; t_R = 16.0 min) to obtain 3 as a white solid, after lyophilization, in 52% yield (143.6 mg, 0.229 mmol). ¹H NMR (500 MHz, CDCl₃) δ 7.82 (d, 2H, Ar), 7.75 (d, 1H, NH), 7.62 (d, 2H, Ar), 7.6 (d, 1H, NH), 5.0 (m, 1H, CH_{ASD}), 4.8 (m, 1H, CH_{Asp}), 2.9 (m, 2H, CH_{2Asp}), 2.7 (m, 2H, CH_{2Asp}), 1.42 (s, 9H, $OC(CH_3)_3$), 1.3 (s, 9H, $OC(CH_3)_3$), 1.1 (s, 18H, $SiC(CH_3)_3$); ¹³C NMR (126 MHz, CDCl₃) δ 171.6, 170.8, 170.0, 169.0, 167.3 (5× C=O), 139.0, 134.3, 134.2, 134.1, 126.1, 82.3, 82.2, 49.7, 37, 36.7, 28, 27.9, 27.2, 20.2, 20.1; ¹⁹F NMR (376 MHz, CDCl₃): δ -188.64; HRMS (ESI/Q-TOF) m/z: [M - H]⁻ calcd for $C_{31}H_{49}$ -FN₂O₈Si 623.3169, found 623.3156.

2-Azido-*N*,*N***-dimethyl-ethanamine** (5). Modified literature protocol was used to perform this reaction. ⁴⁰ 2-Chloro-*N*,*N*-dimethylethanamine hydrochloride (4, 500 mg, 3.47 mmol) was dissolved in deionized water (10 mL), and then sodium azide (677 mg, 10.42 mmol) was added. The mixture was stirred at 80 °C for 40 hours. After cooling, the mixture was adjusted to pH > 9 by the addition of 2 M sodium hydroxide solution (20 mL) and extracted with diethyl ether (60 mL \times 3). The combined extracts were dried over anhydrous sodium sulfate and concentrated to afford compound 5 as colorless oil in 86% yield (339 mg, 2.97 mmol). $R_{\rm f}$ (100% EtOAc) = 0.3;

¹H NMR (500 MHz, CDCl₃) δ 3.29–3.27 (m, 2H), 2.45–2.42 (m, 2H), 2.21–2.19 (m, 6H). ¹³C NMR (126 MHz, CDCl₃) δ 58.0, 48.9, 45.4. HRMS (ESI) m/z: [M + H]⁺ calcd. For C₄H₁₁N₄ 115.0978, found 115.0979.

2-Aminoethyl-(2-azidoethyl)-dimethyl-ammonium chloride (7). *N*-Boc-2-bromoethyl-amine (626 mg, 2.8 mmol) was added to a solution of compound 5 (320 mg, 2.8 mmol) in MeCN (5 mL). The mixture was stirred for 5 days at room temperature to afford 6 which was immediately taken to the deprotection step without further purification. Then, 2 M hydrochloric (1 mL) acid in diethyl ether was added and stirred for 1 hour. White precipitate was formed and filtered off, washed with diethyl ether and dried to afford 7, a white solid, in 71% yield (316 mg, 1.99 mmol). 1 H NMR (500 MHz, D₂O) δ 4.11–4.10 (t, J = 4.5, 2H), 3.89–3.86 (m, 2H), 3.78–3.76 (t, J = 5.5, 2H), 3.69–3.65 (m, 2H), 3.36 (s, 6H). 13 C NMR (125 MHz, D₂O) δ 64.1, 60.9, 52.9, 45.5, 33.8. HRMS (ESI) m/z: $[M^*]^+$ calcd. For $C_6H_{16}N_5$ 158.1406, found 158.1408.

(9S,13S)-Tri-tert-butyl-3,11-dioxo-1-phenyl-2-oxa-4,10,12triazapentadecane-9,13,15-tri-carboxylate (9). To a solution of H-L-Glu(OtBu)-OtBu·HCl (2.42 g, 8.17 mmol) 4-nitrophenyl chloroformate (1.75 g, 8.58 mmol) in CH₂Cl₂ (25 mL), Hünig's base (3.13 mL, 19.97 mmol) was added dropwise at 0 °C. The reaction mixture was stirred for an hour at 0 °C and then allowed to warm to room temperature over 4 additional hours. The reaction mixture was then cooled to 0 °C and H-L-Lys(Z)-OtBu·HCl (2.74 g, 9.40 mmol) was added portionwise, followed by dropwise addition of Hünig's base (3.13 mL, 19.97 mmol). The reaction was then allowed to warm to room temperature over 2 h, followed by dilution with CH₂Cl₂ (80 mL). The resulting organic solution was then washed with NaHCO3 (80 mL × 3), NH4Cl (80 mL), and brine (80 mL), and dried over Na₂SO₄ before being concentrated under vacuum. The crude mixture was purified with flash column chromatography (hexanes/EtOAc gradient, 8:2 → 1: 1) to obtain 9 as a clear oil in 86% yield (4.35 g, 6.99 mmol). $R_{\rm f}$ (hexanes/EtOAc, 4:6) = 0.66. ¹H NMR (500 MHz, CDCl₃) δ 7.4-7.3 (m, 5H, Ar), 5.2-5.0 (m, 4H, CH_2Ph , 2× NH), 4.4-4.3 (m, 2H, 2× CH), 3.2-3.1 (m, 2H, CH₂), 2.28 (m, 2H, CH₂), 2.05 (m, 1H, CH₂), 1.6-1.5 (m, 3H, CH₂), 1.44 (s, 18H, 2× OtBu), 1.42 (s, 9H, OtBu), 1.4-1.3 (m, 2H, CH₂); ¹³C NMR (125 MHz, CDCl₃) δ 172.4, 172.4, and 172.3 (3× C=O_{Ester}), 160.0 $(C=O_{Urea})$, 157.0 (NHCO₂), 136.8 (Ar_{C-C}), 128.5 (2× Ar_{C-H}), 128.1 (Ar_{C-H}), 128.0 ($2 \times$ Ar_{C-H}), 82.9 (C(CH₃)₃), 82.8 (C(CH₃)₃), 81.8 (C(CH_3)₃), 66.6 (CH₂Ph), 54.5 and 54.1 (C_{Lys/Glu^{α}), 40.8} (C_{Lys^e}) , 33.1, 32.5, 28.9, 28.4 (4× CH_2), 28.7 $(C(CH_3)_3)$, 28.3 $(C(CH_3)_3)$, 28.2 $(C(CH_3)_3)$, 23.6 $(C_{LVS'})$; HRMS (ESI) m/z: [M + Na^{+} calcd. For $\text{C}_{32}\text{H}_{51}\text{N}_{3}$ 644.3518, found 644.3516.

1,5-Di-*tert*-butyl (2*S*)-2-{{[(2*S*)-6-amino-1-(*tert*-butoxy)-1-oxohexan-2-yl]carbamoyl}amino)pentanedioate (10). Modified literature protocol was used to perform this reaction. To a solution of 9 (422 mg, 0.679 mmol) in MeOH was added Pd/C. $H_{2(g)}$ was added and bubbled through solution for 5 h. The reaction mixture was filtered through celite and washed with MeOH before concentrating under vacuum. The crude was purified using flash column chromatography (100% CH_2 - $Cl_2 \rightarrow 8:1:1$ $CH_2Cl_2/MeOH/EtOAc + 1\%$ TEA) to obtain 10 as

a pink oil in 88% yield (291 mg, 0.60 mmol). R_f (8:1:1 $CH_2Cl_2/MeOH/EtOAc + 1\% TEA) = 0.3$. 1H NMR (500 MHz, CD_3OD) δ 4.2 (m, 2H, CH_{Lys} , CH_{Glu}), 2.85 (m, 3H, CH_{Lys} , CH_{Glu}), 2.35 (m, 2H, CH_{Glu}), 2.05 (m, 1H, CH_{2Glu}), 1.8 (m, 2H, CH_{2Glu} , CH_{2Lys}), 1.63 (m, 3H, CH_{2Lys}), 1.45 (m, 27H, 3× tBu), 1.25 (m, 2H, CH_{2Lys}); ^{13}C NMR (125 MHz, CD_3OD) δ 173.8 ($C=O_{Ester}$), 173.7 ($C=O_{Ester}$), 173.6 ($C=O_{Ester}$), 160.0 ($C=O_{Urea}$), 82.9 ($C(CH_3)_3$), 82.8 ($C(CH_3)_3$), 81.8 ($C(CH_3)_3$), 54.5 and 54.1 (C_{Lys/Glu^o}), 40.8 (C_{Lys^e}), 33.1, 32.5, 28.9 (3× CH_2), 28.7 ($C(CH_3)_3$), 28.3 ($C(CH_3)_3$), 28.2 ($C(CH_3)_3$), 23.6 (C_{Lys^e}); HRMS (C_{Lys^e}) C_{Lys^e}) C_{Lys^e} (C_{Lys^e}), C_{Lys^e}), C_{Lys^e} 0, 488.333, found 488.3333.

Di-tert-butyl-(2S)-2-[[(1S)-1-tert-butoxycarbonyl-5-(undec-10-ynoylamino)pentyl]carbamoylamino]pentanedioate To a solution of 10 (270 mg, 0.55 mmol) and 10-undecynoic acid (110 g, 0.61 mmol) in dry DMF (2 mL) was added DIPEA (300 μL, 1.65 mmol). After 10 minutes, HBTU (420 mg, 1.1 mmol) was added to the reaction solution and stirred at room temperature overnight. The reaction mixture was concentrated, washed with sat. NaHCO3, H2O and brine, dried over Na2SO4 and concentrated under vacuo. The crude product was purified via flash chromatography (hexanes/ EtOAc, $1:1 \rightarrow 3:7$) to obtain 11 as a white solid in 70% yield $(252 \text{ g}, 0.39 \text{ mmol}). R_f \text{ (EtOAc; } 100\%) = 0.8; {}^{1}\text{H NMR } (498)$ MHz, CDCl₃) δ 5.79 (t, 1H, NH_{Amide}), 5.12 (d, 2H, 2 × NH_{Urea}), 4.31 (m, 2H, $2 \times CH_{Lys/Glu^{\alpha}}$), 3.23 (m, 2H, $CH_{2Lys^{\epsilon}}$), 2.31 (m, 2H, $CH_{2Glu^{\gamma}}$), 2.17 (m, 4H, 2× CH_{2Alkyl}), 2.08 (m, 1H, $CH_{2Glu^{\beta}}$), 1.93 (t, 1H, CH_{Alkyne}), 1.80 (m, 3H, $CH_{2Glu/Lys^{\beta}}$), 1.62 (m, 3H, $CH_{2Lys^{5/8}}$, 1.50-1.69 (m, 4H, $CH_{2Lys^{8}/Alkyl}$), 1.47 (s, 9H, OtBu), 1.47 (s, 9H, OtBu), 1.45 (s, 9H, OtBu), 1.30-1.41 (m, 9H, CH_{2Alkyl}); 13 C NMR (125 MHz, CDCl₃) δ 173.4, 172.4, 172.4, 172.3, 156.6 (5× C=O), 84.8 (C_{Alkyne}), 82.1 (C(CH₃)₃), 81.8 $(C(CH_3)_3)$, 80.6 $(C(CH_3)_3)$, 68.1 (CH_{Alkyne}) , 53.3 and 53.0 $(C_{Lys/Glu^{\alpha}})$, 38.9, 36.8, 32.6, 31.6, 29.3, 29.2, 29.0, 28.9, 28.7, 28.5 and 28.3 (11× CH₂), 28.1 ($C(CH_3)_3$), 28.0 (2× $C(CH_3)_3$), 25.8 (CH_{2Alkyl}), 22.2 (CH_{2Lys}), 18.4 (CH_{2Alkyl}); HRMS (ESI/Q-TOF) m/z: $[M + Na]^+$ calcd for $C_{35}H_{61}N_3O_8Na$ 674.4351, found 674.4348.

 $(2-Azidoethyl)({2-[(2R)-4-(tert-butoxy)-2-[(2R)-4-(t$ butoxy)-2-({4-[di-tert-butyl(fluoro)silyl]phenyl}formamido)-4oxobutanamido]-4-oxobutanamido]ethyl})dimethylazanium chloride (12). To a solution of 3 (47.5 mg, 0.076 mmol) and 7 (21.9 mg, 0.095 mmol) in dry DMF (2 mL) at room temperature was added DIPEA (0.06 mL, 0.323 mmol). The solution was sonicated to get white precipitate into solution. After 10 min, HBTU (61.8 mg, 0.152 mmol) was added. After 24 h total reaction time, the reaction solution was diluted with hexanes and EtOAc and concentrated in vacuo. Toluene was added and removed 3× in vacuo to remove DMF. The crude mixture was purified via HPLC (Polar C18 column: Luna Omega 5 μ m 100 Å 250 mm \times 10 mm; flow: 2.5 mL min⁻¹; solvent A: H₂O, solvent B: MeCN + 0.1% TFA, method: 0-4 min isocratic 50% B; 4-15 min linear gradient → 95% B, 15-25 min isocratic 95% B; t_R = 16.8 min) to obtain 12 as a white powder in 83% yield (50.7 mg, 0.063 mmol). ¹H NMR (700 MHz, CD₃OD) δ 7.90 (d, 2H, J = 8.40 Hz, Ar), 7.75 (d, 2H,

J = 8.40 Hz, Ar), 4.89 (dd, 1H, J = 2.10, 5.60 Hz, CH_{Aspa}, 4.63 (t, 1H, J = 6.30 Hz, CH_{Aspa}, 3.97 (m, 2H, CH₂), 3.70 (m, 2H, CH₂), 3.60 (m, 2H, CH₂), 3.55 (m, 2H, CH₂), 3.35 (m, 3H, NH), 3.19 (s, 6H, 2× CH₃), 2.97 (dd, 1H, J = 5.59, 10.49 Hz, CH_{2Aspa}, 2.77 (m, 3H, CH_{2Aspa}, 1.46 (s, 9H, OC(CH₃)₃), 1.37 (s, 9H, OC(CH₃)₃), 1.07 (s, 18H, 2× SiC(CH₃)₃); ¹³C NMR (126 MHz, CD₃OD) δ 173.3, 173.0, 171.9, 171.8, and 170.6 (5× C=O), 139.1 (Ar_{C-Si}, ${}^2J_{C,F}$ = 13.7 Hz), 135.9 (Ar_{C-C}), 135.3 (Ar_{C-H}, ${}^3J_{C,F}$ = 4.1 Hz), 127.7 (Ar_{C-H}), 82.7 and 82.6 (2× OC(CH₃)₃), 64.4 and 64.2 (2× NCH₂), 52.5 and 52.4 (2× N(CH₃)) 51.6 and 49.5 (2× CH_{Aspa}, 45.9 (N₃CH₂), 37.6 and 37.2 (2× CH_{2Aspa}, 34.9 (NHCH₂), 28.4 and 28.3 (2× OC(CH₃)₃), 27.7 (2× SiC(CH₃)₃), 21.0 (2× SiC(CH₃)₃, ${}^2J_{C,F}$ = 12.1 Hz); HRMS (ESI/Q-TOF) m/z: [M⁺] calcd for C₃₇H₆₃FN₇O₇Si 764.4537, found 764.4534.

 ${2-[(2R)-3-Carboxy-2-[(2R)-3-carboxy-2-(\{4-[di-tert-butyl-x]-x]-(x)-x]}$ (fluoro)silyl]phenyl}formamido)propanamido]propanamido]ethyl}({2-[4-(8-{[(5S)-5-carboxy-5-({[(1S)-1,3-dicarboxypropyl]carbamoyl\amino)pentyl]carbamoyl\octyl)-1H-1,2,3-triazol-1yl]ethyl})dimethylazanium trifluoroacetate (PSiMA) (14). To a solution of 12 (59 mg, 0.07 mmol) and 11 (62.5 mg, 0.10 mmol) in THF (2 mL) was added CuSO₄ (12.5 mg, 0.08 mmol), sodium ascorbate (10 mg, 0.05 mmol) and 12 drops of deionized H2O. A small amount of deionized water was necessary to solubilize reagent copper and facilitate interaction with the starting materials. Once the starting material had mostly been consumed (TLC monitoring), the crude was resuspended in 1:1 CH₂Cl₂/TFA (4 mL), without purification. The reaction mixture was stirred for 24 h at room temperature. The crude mixture was concentrated then purified via HPLC (C18(2) column: Luna 5 μm 100 Å 250 mm × 10 mm; flow: 2.5 mL min⁻¹; solvent A: H₂O, solvent B: MeCN + 0.1% TFA, method: isocratic 45% B; $t_{\rm R}$ = 16 min) to obtain 14 as a white powder, after lyophilization, in 20% yield (17.1 mg, 0.015 mmol). ¹H NMR (500 MHz, CD₃OD) δ 7.92 (s, 1H, 7.90, $CH_{Triazole}$), 7.87 (d, 2H, J = 8.0 Hz, Ar), 7.73 (d, 2H, J = 8.0Hz, Ar), 4.99 (t, 2H, J = 6.5 Hz, $CH_{2Triazole}$), 4.87 (t, 1H, J = 6.5Hz, $CH_{Asp^{\alpha}}$), 4.67 (t, 1H, J = 6.0 Hz, $CH_{Asp^{\alpha}}$), 4.30 (dd, 1H, J = 3, 5.5, $CH_{Glu^{\alpha}}$), 4.24 (dd, 1H, J = 3.5, 4.5, $CH_{Lys^{\alpha}}$), 3.70 (m, 2H, CH₂), 3.61 (m, 2H, CH₂), 3.18 (s, 6H, 2× NCH₃), 3.16 (m, 2H, CH_2), 3.03 (dd, 1H, J = 7, 9.5 Hz, CH_2), 2.85 (m, 3H, CH_2), 2.70 $(t, 2H, J = 7.5 \text{ Hz}, CH_2), 2.41 \text{ (m, 2H, CH_2)}, 2.15 \text{ (m, 3H, CH_2)},$ 1.86 (m, 2H, CH₂), 1.67 (m, 3H, CH₂), 1.61–1.39 (m, 6H, CH₂), 1.32 (m, 8H, CH₂), 1.06 (s, 18H, 2× SiC(CH₃)₃); ¹³C NMR (126 MHz, CD₃OD) δ 176.6, 176.5, 176.3, 175.9, 175.3, 174.5, 173.7, 173.4, 170.5, 160.1 (10× C=O), 150.2 (C_{Triazole}), 139.8 (Ar_{C-Si}, $^{2}J_{C,F}$ = 13.4 Hz), 136.1 (Ar_{C-C}), 135.2 (Ar_{C-H}, $^{3}J_{C,F}$ = 4.2 Hz), 127.6 (Ar_{C-H}), 124.1 (CH_{Triazole}), 64.5, 63.7 (2× NCH₂), 54.1, 53.6 (2× $CH_{2Asp^{\alpha}}$), 52.5 (2× $N(CH_3)$), 52.3, 51.5 (2× $CH_{Lys/Glu^{\alpha}}$), 49.7 (CH₂) 44.7 (CH_{2Triazole}), 40.0 (CH_{2Lys^e}), 37.1, 36.0 (2× CH_{2Asp}), 34.9 (CH_2) , 33.2 $(CH_{Lvs^{\beta}})$, 31.1 $(CH_{2Glu^{\gamma}})$, 30.3, 30.2, 30.1, 30.1, 30.0, 29.9 (6× CH₂), 28.9 (CH_{2Gluβ}), 27.7, 27.0 (2× CH_2), 26.2 (2× $SiC(CH_3)_3$), 24.0 (CH_2), 21.0 (2× $SiC(CH_3)_3$, ${}^2J_{C.F.}$ = 12.1 Hz); ¹⁹F NMR (376 MHz, CD₃OD): δ -189.46, -76.9 (TFA); HRMS (ESI/Q-TOF) m/z: $[M^*]^+$ calcd for $C_{52}H_{84}FN_{10}O_{15}$ -Si 1135.5865, found 1135.5860.

Radiochemical synthesis of 18 F-PSiMA. Low A_m method: the [18F]fluoride was supplied by the Edmonton Radiopharmaceutical Centre (ERC) in quantities of 1-1.5 GBq in \sim 2 mL. The 4 drop method was then utilized, passing the [18F]fluoride in cyclotron water through the male end of a OMA cartridge (Sep-Pak Accell Plus OMA Carbonate Plus Light (46 mg) cartridge) using a male-to-female adaptor. 29,36 Two times 10 mL of air were then passed through the QMA cartridge. The cartridge was then reversed and four drops of an elution solution (K222 (7-9 mg), K2CO3 (1 M, 10 μ L), H2O (40 μL) and MeCN (900 μL)) were eluted into a drying vial. The resulting elution efficiency was determined to be 67 \pm 8% (amount of activity eluted vs. trapped on cartridge). The vial containing [18F]fluoride and 4 drops of elution solution was put into an oil bath at 80 °C under a stream of N2. Anhydrous MeCN (3 × 1 mL) was added every 5 minutes. A solution of precursor 14 (20 nmol in 200 µL dry MeCN), was added to the drying vial containing [18F]fluoride and allowed to sit at room temperature for 10 min. The reaction mixture was then diluted with HPLC solvent (250 µL MeCN + 0.1% TFA and 550 μ L H₂O + 0.1% TFA, 1 mL) and semipreparative radioHPLC was used for purification (C18(2) column: Luna 5 μm 100 Å 250 mm × 10 mm; flow: 2.0 mL min⁻¹; solvent A: H₂O + 0.1% TFA, solvent B: MeCN + 0.1% TFA, method: isocratic 45% B; $t_{\rm R}$ = 16 min). The fraction collected at 16 min was diluted with 12 mL H₂O then passed through an Oasis cartridge (Waters Oasis Light HLB cartridge), dried with 2 × 10 mL air, the eluted with 10 drops of EtOH. The EtOH was removed by evaporation (85 °C for 10 min) and resuspended in 0.9% saline with 10% polyethylene glycol as an injectable solution or Krebs buffer for cell studies. 18F-PSiMA was synthesized with an RCC of $68 \pm 12\%$ (n = 6), as determined by HPLC through analyzing the area under the curve (AUC) for the free F-18 peak and product peak. The non-decay corrected RCY of 18 F-PSiMA was 13 \pm 8% (n = 6), measured after purification and formulation. Total reaction time from time of drying to formulation, including radiolabeling and HPLC purification, was 90 min. The $A_{\rm m}$ at the end of synthesis was $10.93 \pm 3.70 \text{ GBq } \mu\text{mol}^{-1}$, determined by HPLC calibration curve. Quality control was performed by radioHPLC, confirming the product was prepared in >99% RCP. High A_m method: 4.10 GBq of [18 F] fluoride in cyclotron water was passed through the male end of a QMA cartridge (Sep-Pak Accell Plus QMA Carbonate Plus Light (46 mg) cartridge) using an female-to-female Luer adaptor. 10 mL of air was then passed through the QMA cartridge, and the cartridge was then reversed and the first four drops of an elution solution (K222 (8.6 mg), K2CO3 (1 M, 10 μL), H₂O (40 μL), and MeCN (900 μL)) were eluted into a V-vial. The [18F]fluoride solution was put into an oil bath at 110 °C and dried under a stream of N2 for 30 min. The resulting residue was resuspended in anhydrous MeCN (25 μL) and added to a small pre-heated (80 °C) V-vial containing precursor 14 (5 nmol). The drying vial was washed again with MeCN (25 µL) and added to the reaction vial. The reaction vial was removed from heat and the exchange reaction was

allowed to proceed at room temperature for 15 min. The reaction vial was then diluted with HPLC eluent (45% MeCN in H₂O, 0.5 mL) and injected onto HPLC (C18(2) column: Luna 5 μ m 100 Å 250 mm × 10 mm; flow: 3.0 mL min⁻¹; solvent A: H₂O + 0.2% TFA, solvent B: MeCN, method: isocratic 45% B; $t_{\rm R}$ = 11.5 min). The fraction collected at 11.5 min was diluted with H2O (20 mL) and passed through a Waters Oasis Light HLB cartridge, washed with H₂O (3 mL), and then dried with 10 mL air. ¹⁸F-PSiMA was eluted in 12 drops of EtOH, which was concentrated down to ~20 μL under a stream of N2 while heating to 90 °C. ¹⁸F-PSiMA (322 MBq delivered activity, $A_{\rm m} = 82.54 \text{ GBq } \mu\text{mol}^{-1}$) was synthesized over 70 min (from start of drying to delivery to the microPET facility) with a non-decay corrected radiochemical yield of 7.9%. The RCP was >99%, as determined by radioHPLC.

In vitro cell uptake and competitive displacement studies. LNCaP cells were cultured in RPMI-1640 supplemented with 10% fetal bovine serum and 1% penicillin/streptomycin. Cell uptake experiments were performed over 120 min incubation time. LNCaP cells were initially seeded in d in poly-D-lysine-coated 12-well plates and incubated for 48 h reaching 95% confluency. The medium was subsequently removed 1 h before the assay, and the cells were rinsed twice with PBS. Next, 300 µL Krebs-Ringer buffer solution (120 mM NaCl, 4 mM KCl, 1.2 mM KH₂PO₄, 2.5 mM, MgSO₄, 25 mM NaHCO₃, 70 µM CaCl₂, pH 7.4) was added to each well. Then 0.2 MBq of 18F-PSiMA was added to each well, and the plate was kept at 5% CO2 incubator at 37 °C for the different time points. Radiotracer uptake was stopped with 1 mL of ice-cold PBS, and the cells were washed twice with PBS and lysed in 0.3 mL radioimmunoprecipitation assay buffer (RIPA buffer). Radioactivity in 300 µL of cell lysates was determined as Becquerel [Bq] using a HIDEX automated γ-counter (Hidex Oy, Turku, Finland). Total protein concentration in the samples was determined by the bicinchoninic acid method (BCA 23227; Pierce, Thermo Scientific) using bovine serum albumin as protein standard. Data were calculated as percent of measured radioactivity per milligram of protein (% radioactivity per mg of protein). Graphs were constructed using GraphPad Prism 5.0 (GraphPad Software, San Diego, CA). For competitive displacement experiments increasing concentrations (10⁻¹⁰ to 10⁻⁴ M) of either precursor 14 or 2-(phosphonomethyl)pentanedioic acid (2-PMPA, Sigma-Aldrich, St. Louis, MO, USA) were added to the wells shortly before radiotracer addition. After 60 min radiotracer uptake was stopped, cell lysed and counted as described above. For internalization experiments cellular uptake was also stopped by removing incubation media from the cells and washing the wells twice with icecold PBS buffer (1 mL). Surface-bound radioactivity was removed from the cells through incubating the cells twice with 0.5 mL glycine-HCl in PBS (50 mM, pH 2.5) for 5 min at 37 °C. Cells were washed again with ice-cold PBS before the addition of RIPA buffer (400 µL) to lyse the cells. Cells were returned into the incubator for 10 min, and cell lysates were collected and counted as described above.

Animal studies. All animal experiments were carried out in accordance with the guidelines of the Canadian Council on Animal Care (CCAC) and approved by the local animal care committee (Cross Cancer Institute, University of Alberta). PET imaging experiments were carried out in male tumor-bearing nu/nu mice (Charles Laboratories, Quebec, Canada). LNCaP (15-20 × 10⁶ cells in 200 μL of matrigel/PBS 50/50) were injected into the upper left flank of these mice (20-24 g). Before injecting LNCaP cells, the mice received a 1.0 mg per pellet containing dehydroepiandrosterone (DHEA) in a 60-day release preparation (Innovative Research of America, Sarasota, FL, USA). The pellet was implanted subcutaneously into the upper right flank in order to provide a constant level of testosterone to support tumor growth of androgen receptorpositive LNCaP cells. Tumors reached sizes of approximately 7×7 mm which were suitable for PET experiments.

Research Article

Dynamic PET imaging. General anesthesia of LNCaP tumor-bearing mice was induced with inhalation of isoflurane in 40% oxygen/60% nitrogen (gas flow 1 mL min⁻¹), and the mice were subsequently fixed in prone position. The body temperature was kept constant at 37 °C for the entire experiment. The mice were positioned in a prone position into the center of the field of view of an INVEON® PET/CT scanner (Siemens Preclinical Solutions, Knoxville, TN). A transmission scan for attenuation correction was not acquired. The mice were injected with 4-6 MBq of ¹⁸F-PSiMA in 100-150 μL of isotonic NaCl solution (0.9%) through a tail vein catheter. For blocking studies, the animals were pre-dosed with 300 µg of DCFPyL in 50 µL saline about 5 min before radiotracer injection. Data acquisition was performed over 60 min in a 3D list mode. The dynamic list mode data were sorted into sinograms with 54 time frames (10 \times 2, 8 \times 5, 6 \times 10, 6×20 , 8×60 , 10×120 , 6×300 s). The frames were reconstructed using maximum a posteriori (MAP) as reconstruction mode. The pixel size was 0.085 × 0.085 × 0.121 mm³ (256 \times 256 \times 63), and the resolution in the center of the field of view was 1.8 mm. No correction for partial volume effects was applied. The image files were processed using the ROVER v 2.0.51 software (ABX GmbH, Radeberg, Germany). Masks defining 3D regions of interest (ROI) were set and defined by thresholding. Mean standardized uptake values (SUV_{mean} as activity per mL tissue)/(injected activity per body weight), mL g⁻¹, were determined for each ROI. Time-activity curves (TACs) were generated for the dynamic scans. All semi-quantified PET data are presented as means ± SEM from n experiments.

Radiometabolite analysis. Healthy BALB/c mice were injected with \sim 20 MBq of ¹⁸F-PSiMA. Venous blood samples were collected at 5, 15, 30, and 60 min p.i. via the mouse tail vein and further processed. Blood cells were separated by centrifugation (13 000 rpm × 5 min). Precipitation of proteins in the supernatant was achieved by the addition of 2 volume parts of MeOH, and the samples were centrifuged again (13 000 rpm for 5 min) to obtain the protein and plasma fraction.

Fractions of blood cells, proteins, and plasma were measured using a HIDEX automated γ-counter (Hidex Oy, Turku, Finland) to determine radioactivity per sample. The clear plasma supernatant was injected into a Shimadzu HPLC system. The samples were analyzed by radioHPLC (C18(2) column: Luna 10 µm 100 Å 250 mm × 4.6 mm; flow: 1.0 mL min⁻¹; solvent A: H₂O + 0.2% TFA, solvent B: MeCN, method: 0-3 min 10% B, 10 min 30% B, 17 min 50% B, 23 min 70% B, 27-30 min 90% B).

Lipophilicity determination. To the lyophilized ¹⁹F-PSiMA (50 nmol) was added 1-octanol (500 µL) and 100 mM PBS pH 7.4 (50 µL). The biphasic mixture was vigorously agitated for 1 minute at room temperature, and the octanol and aqueous phases were separated by centrifugation for 5 minutes. The aliquot of an octanol phase was diluted with DMF (1:1) to reduce the viscosity, while the aliquot of an aqueous phase was diluted with PBS (1:19) to decrease the concentration. The samples were analyzed by HPLC to measure concentrations of the analyte and the $\log D$ of ¹⁹F-PSiMA was calculated as $log(C_{octanol}/C_{water})$ factoring the ratio of solvents and dilutions of each phase. The measurement was repeated

Hydrolytic stability assay. A solution of 19F-PSiMA in aqueous PBS at pH 7.4 (100 µM) was incubated in a thermostated autosampler at 37 °C. The hydrolysis rate was monitored by HPLC equipped with a UV detector (monitoring at 230 nm) for 4 days and a single hydrolysis product was observed. The half-life of the first-order hydrolysis was calculated from the semi-logarithmic plots of intact 19F-PSiMA (log %) against time with excellent linear regression fit ($R^2 > 0.99$). The measurement was repeated in duplicate.

Data availability

The data supporting this article have been included as part of the ESI.†

Author contributions

Lexi Gower-Fry: investigation, data curation, formal analysis, methodology, validation, visualization, writing. Justin J. Bailey: conceptualization, methodology, validation, investigation, formal analysis, writing. Melinda Wuest: investigation, formal analysis, writing, visualization. Susan Pike: investigation. Alexey Kostikov: investigation, writing. Dorian: investigation. Andreas Carmen Wängler: conceptualization, writing. Frank Wuest, Ralf Schirrmacher: conceptualization, funding acquisition, writing, supervision.

Conflicts of interest

There are no conflicts to declare.

Acknowledgements

This research was funded by the Natural Science and Engineering Research Council of Canada (individual

operating grant to RS) and the New Frontiers in Research Fund (grant NFRFT-2022-00269, to RS). This manuscript is dedicated to Prof. Dr. Klaus Jurkschat in profound recognition of his invaluable contributions advancement of SiFA radiochemistry. The authors would like to thank members of Dr. Frank Wuest's research group; Dr. Jenilee Woodfield, Jennifer Dufour, and Cody Bergman, for their assistance with the radiosynthesis, cell culture and in vitro cell experiments. The authors would also like to thank the Edmonton Radiopharmaceutical Centre (ERC) for ¹⁸F radionuclide production and for providing ¹⁸F-PSMA-1007 as well as the Vivarium at the Cross Cancer Institute for supporting the animal studies. In addition, the authors would like to thank members of Dr. Ralf Schirrmacher's group, specifically Yinglan Pu, Dr. Carolin Jaworski and Travis Kronemann for their assistance with the organic synthesis. Finally, we would like to thank the Alberta Cancer Foundation (ACF) for their financial support of this work.

Notes and references

- 1 L. Evangelista, F. Zattoni, G. Cassarino, P. Artioli, D. Cecchin, F. Dal Moro and P. Zucchetta, Eur. J. Nucl. Med. Mol. Imaging, 2021, 48, 859-873.
- 2 M. A. Hoffmann, H. J. Wieler, C. Baues, N. J. Kuntz, I. Richardsen and M. Schreckenberger, Urology, 2019, 130,
- 3 S. Houshmand, C. Lawhn-Heath and S. Behr, *Abdom. Radiol.*, 2023, 48, 3610-3623.
- 4 M. Weber, C. Kurek, F. Barbato, M. Eiber, T. Maurer, M. Nader, B. Hadaschik, V. Grünwald, K. Herrmann, A. Wetter and W. P. Fendler, J. Nucl. Med., 2021, 62, 88-91.
- 5 J. Cardinale, M. Schäfer, M. Benešová, U. Bauder-Wüst, K. Leotta, M. Eder, O. C. Neels, U. Haberkorn, F. L. Giesel and K. Kopka, J. Nucl. Med., 2017, 58, 425-431.
- 6 Y. Chen, M. Pullambhatla, C. A. Foss, Y. Byun, S. Nimmagadda, S. Senthamizhchelvan, G. Sgouros, R. C. Mease and M. G. Pomper, Clin. Cancer Res., 2011, 17, 7645-7653.
- 7 M. Eiber, W. P. Fendler, S. P. Rowe, J. Calais, M. S. Hofman, T. Maurer, S. M. Schwarzenboeck, C. Kratowchil, K. Herrmann and F. L. Giesel, J. Nucl. Med., 2017, 58, 67S-76S.
- 8 Z. Zhang, Z. Zhu, D. Yang, W. Fan, J. Wang, X. Li, X. Chen, Q. Wang and X. Song, Oncol. Lett., 2016, 12, 1001-1006.
- 9 U. Hennrich and M. Eder, *Pharmaceuticals*, 2021, 14, 713.
- 10 S. P. Rowe, K. J. Macura, E. Mena, A. L. Blackford, R. Nadal, E. S. Antonarakis, M. Eisenberger, M. Carducci, H. Fan, R. F. Dannals, Y. Chen, R. C. Mease, Z. Szabo, M. G. Pomper and S. Y. Cho, Mol. Imaging Biol., 2016, 18, 411-419.
- 11 M. Kroenke, L. Schweiger, T. Horn, B. Haller, K. Schwamborn, A. Wurzer, T. Maurer, H.-J. Wester, M. Eiber and I. Rauscher, J. Nucl. Med., 2022, 63, 1809–1814.
- 12 M. A. Green, G. D. Hutchins, C. D. Bahler, M. Tann, C. J. Mathias, W. Territo, J. Sims, H. Polson, D. Alexoff, W. C. Eckelman, H. F. Kung and J. W. Fletcher, Mol. Imaging Biol., 2020, 22, 752-763.

- 13 W. Cytawa, A. K. Seitz, S. Kircher, K. Fukushima, J. Tran-Gia, A. Schirbel, T. Bandurski, P. Lass, M. Krebs, W. Połom, M. Matuszewski, H.-J. Wester, A. K. Buck, H. Kübler and C. Lapa, Eur. J. Nucl. Med. Mol. Imaging, 2020, 47, 168-177.
- 14 S. C. Behr, R. Aggarwal, H. F. Vanbrocklin, R. R. Flavell, K. Gao, E. J. Small, J. Blecha, S. Jivan, T. A. Hope, J. P. Simko, J. Kurhanewicz, S. M. Noworolski, N. J. Korn, R. De Los Santos, M. R. Cooperberg, P. R. Carroll, H. G. Nguyen, K. L. Greene, B. Langton-Webster, C. E. Berkman and Y. Seo, J. Nucl. Med., 2019, 60, 910-916.
- 15 F. Dietlein, M. Hohberg, C. Kobe, B. D. Zlatopolskiy, P. Krapf, H. Endepols, P. Täger, J. Hammes, A. Heidenreich, B. Neumaier, A. Drzezga and M. Dietlein, J. Nucl. Med., 2020, 61, 202-209.
- 16 T. Saga, Y. Nakamoto, T. Ishimori, T. Inoue, Y. Shimizu, H. Kimura, S. Akamatsu, T. Goto, H. Watanabe, K. Kitaguchi, M. Watanabe, M. Ono, H. Saji, O. Ogawa and K. Togashi, Cancer Sci., 2019, 110, 742-750.
- 17 X. Li, M. Yu, J. Yang, D. Li, R. Li, J. Mao, C. Zuo, Z. Liang, Q. Li and C. Cheng, EJNMMI Rep., 2024, 8(1), 28.
- 18 C. Wängler, L. Beyer, P. Bartenstein, B. Wängler, R. Schirrmacher and S. Lindner, EJNMMI Radiopharm. Chem., 2022, 7, 22.
- 19 M. Unterrainer, S. C. Kunte, L. M. Unterrainer, A. Holzgreve, A. Delker, S. Lindner, L. Beyer, M. Brendel, W. G. Kunz, M. Winkelmann, C. C. Cyran, J. Ricke, K. Jurkschat, C. Wängler, B. Wängler, R. Schirrmacher, C. Belka, M. Niyazi, J.-C. Tonn, P. Bartenstein and N. L. Albert, Eur. J. Nucl. Med. Mol. Imaging, 2023, 50, 3390-3399.
- 20 R. S. Eschbach, M. Hofmann, L. Späth, G. T. Sheikh, A. Delker, S. Lindner, K. Jurkschat, C. Wängler, B. Wängler, R. Schirrmacher, R. Tiling, M. Brendel, V. Wenter, F. J. Dekorsy, M. J. Zacherl, A. Todica, H. Ilhan, F. Grawe, C. C. Cyran, M. Unterrainer, J. Rübenthaler, T. Knösel, T. Paul, S. Boeck, C. B. Westphalen, C. Spitzweg, C. J. Auernhammer, P. Bartenstein, L. M. Unterrainer and L. Beyer, Front. Oncol., 2023, 13, 992316.
- 21 C. Wängler, S. Niedermoser, J. Chin, K. Orchowski, E. Schirrmacher, K. Jurkschat, L. Iovkova-Berends, A. P. Kostikov, R. Schirrmacher and B. Wängler, Nat. Protoc., 2012, 7, 1946-1955.
- 22 S. Lindner, C. Wängler, J. J. Bailey, K. Jurkschat, P. Bartenstein, B. Wängler and R. Schirrmacher, Nat. Protoc., 2020, 15, 3827-3843.
- 23 H. Ilhan, S. Lindner, A. Todica, C. C. Cyran, R. Tiling, C. J. Auernhammer, C. Spitzweg, S. Boeck, M. Unterrainer, F. J. Gildehaus, G. Böning, K. Jurkschat, C. Wängler, B. Wängler, R. Schirrmacher and P. Bartenstein, Eur. J. Nucl. Med. Mol. Imaging, 2020, 47, 870-880.
- 24 S. Lindner, M. Simmet, F. Gildehaus, K. Jurkschat, C. Wängler, B. Wängler, P. Bartenstein, R. Schirrmacher and H. Ilhan, Nucl. Med. Biol., 2020, 88-89, 86-95.
- 25 M. Unterrainer, S. Lindner, L. Beyer, F. Gildehaus, A. Todica, L. Mittlmeier, K. Jurkschat, C. Wängler, B. Wängler, R. Schirrmacher, J. Tonn, N. Albert, P. Bartenstein and H. Ilhan, Clin. Nucl. Med., 2021, 46(8), 667-668.

26 L. Beyer, A. Gosewisch, S. Lindner, F. Völter, L. M. Mittlmeier, R. Tiling, M. Brendel, C. C. Cyran, M. Unterrainer, J. Rübenthaler, C. J. Auernhammer, C. Spitzweg, G. Böning, F. J. Gildehaus, K. Jurkschat, C. Wängler, B. Wängler, R. Schirrmacher, V. Wenter, A. Todica, P. Bartenstein and H. Ilhan, Eur. J. Nucl. Med. Mol. Imaging, 2021, 48, 3571-3581.

Research Article

- 27 S. Niedermoser, J. Chin, C. Wängler, A. Kostikov, V. Bernard-Gauthier, N. Vogler, J.-P. Soucy, A. J. Mcewan, R. Schirrmacher and B. Wängler, J. Nucl. Med., 2015, 56, 1100-1105.
- S. C. Kunte, L. M. Unterrainer, W. G. Kunz, M. Winkelmann, S. Lindner, K. Jurkschat, C. Wängler, B. Wängler, R. Schirrmacher, P. Bartenstein, C. Belka, C. Schichor, N. L. Albert and M. Unterrainer, Clin. Nucl. Med., 2024, 49(12), e689-e690.
- 29 J. Bailey, M. Wuest, M. Wagner, A. Bhardwaj, C. Wängler, B. Wängler, J. Valliant, R. Schirrmacher and F. Wuest, J. Med. Chem., 2021, 64(21), 15671-15689.
- 30 A. Kostikov, L. Iovkova, J. Chin, E. Schirrmacher, B. Wängler, C. Wängler, K. Jurkschat, G. Cosa and R. Schirrmacher, J. Fluorine Chem., 2011, 132(1), 27-34.
- 31 S. Litau, S. Niedermoser, N. Vogler, M. Roscher, R. Schirrmacher, G. Fricker, B. Wängler and C. Wängler, Bioconjugate Chem., 2015, 26(12), 2350-2359.

- 32 C. Wängler, A. Kostikov, J. Zhu, J. Chin, B. Wängler and R. Schirrmacher, Appl. Sci., 2012, 2, 277-302.
- 33 A. Kozikowski, F. Nan, P. Conti, J. Zhang, E. Ramadan, T. Bzdega, B. Wroblewska, J. Neale, S. Pshenichkin and J. Wroblewski, J. Med. Chem., 2001, 44(3), 298-301.
- 34 A. Kozikowski, J. Zhang, F. Nan, P. Petukhov, E. Grajkowska, J. Wroblewski, T. Yamamoto, T. Bzdega, B. Wroblewska and J. Neale, J. Med. Chem., 2004, 47(7), 1729-1738.
- 35 M. Wirtz, A. Schmidt, M. Schottelius, S. Robu, T. Günther, M. Schwaiger and H.-J. Wester, EJNMMI Res., 2018, 8(1), 84.
- 36 D. Connolly, J. Bailey, H. Ilhan, P. Bartenstein, C. Wängler, B. Wängler, M. Wuest, F. Wuest and R. Schirrmacher, J. Visualized Exp., 2020, 155, e60623.
- 37 S. Robu, A. Schmidt, M. Eiber, M. Schottelius, T. Günther, B. H. Yousefi, M. Schwaiger and H.-J. Wester, EJNMMI Res., 2018, 8(1), 30.
- 38 A. Wurzer, M. Parzinger, M. Konrad, R. Beck, T. Günther, V. Felber, S. Färber, D. Di Carlo and H.-J. Wester, EJNMMI Res., 2020, 10(1), 149.
- 39 V. Bouvet, M. Wuest, J. J. Bailey, C. Bergman, N. Janzen, J. F. Valliant and F. Wuest, Mol. Imaging Biol., 2017, 19, 923-932.
- 40 Y. Yuan, W. Wu, S. Xu and B. Liu, Chem. Commun., 2017, 53, 5287-5290.